Environmental Science and Engineering

Long Quoc Nguyen
Luyen Khac Bui
Xuan-Nam Bui
Hai Thanh Tran *Editors*

Advances in Geospatial Technology in Mining and Earth Sciences

Selected Papers of the 2nd International Conference on Geo-spatial Technologies and Earth Resources 2022

Springer

Environmental Science and Engineering

The ultimate goal of this series is to contribute to the protection of our environment, which calls for both profound research and the ongoing development of solutions and measurements by experts in the field. Accordingly, the series promotes not only a deeper understanding of environmental processes and the evaluation of management strategies, but also design and technology aimed at improving environmental quality. Books focusing on the former are published in the subseries Environmental Science, those focusing on the latter in the subseries Environmental Engineering.

Long Quoc Nguyen · Luyen Khac Bui ·
Xuan-Nam Bui · Hai Thanh Tran
Editors

Advances in Geospatial Technology in Mining and Earth Sciences

Selected Papers of the 2nd International Conference on Geo-spatial Technologies and Earth Resources 2022

Springer

Editors
Long Quoc Nguyen
Department of Mine Surveying
Hanoi University of Mining and Geology
Hanoi, Vietnam

Luyen Khac Bui
Department of Geodesy
Hanoi University of Mining and Geology
Hanoi, Vietnam

Xuan-Nam Bui
Department of Surface Mining
Hanoi University of Mining and Geology
Hanoi, Vietnam

Hai Thanh Tran
Department of Geology
Hanoi University of Mining and Geology
Hanoi, Vietnam

ISSN 1863-5520 ISSN 1863-5539 (electronic)
Environmental Science and Engineering
ISBN 978-3-031-20462-3 ISBN 978-3-031-20463-0 (eBook)
https://doi.org/10.1007/978-3-031-20463-0

This Springer imprint is published by the registered company Springer Nature Switzerland AG
The registered company address is: Gewerbestrasse 11, 6330 Cham, Switzerland

Preface

This book comprises a series of selected high-quality peer-reviewed papers delivered at the 2nd International Conference on Geospatial Technologies and Earth Resources (GTER 2022). The event will be held during October 14–15, 2022, at Hanoi University of Mining and Geology (HUMG), Hanoi, Vietnam, which is co-organized by HUMG and the International Society for Mine Surveying (ISM) to celebrate the 55th anniversary of the Department of Mine Surveying (HUMG). The conference is financially supported by the Vietnam Mining Science and Technology Association (VMSTA), the Vietnam Association of Geodesy, Cartography and Remote Sensing (VGCR), Vietnam National Coal-Mineral Industries Holding Corporation Limited (VINACOMIN), and Dong Bac Corporation (NECO).

The conference is believed to be an excellent opportunity during the COVID pandemic for the authors and participants to discuss advanced technologies and scientific directions in the fields of geospatial technologies and earth resources. Additionally, via this conference, a chance to exchange new ideas, innovative thinking, and application experiences both virtual and in-person will be provided, by which research or business relations and partner finding for future collaborations would have been established.

Totally, 205 manuscripts have been submitted to the organizing committee. Subsequently, after screening by the selection committee and reviewing by at least two blind reviewers, 34 research and review papers have been selected to be presented at the conference. The selected papers will be delivered over four planned sessions covering different topics of geospatial technologies, earth sciences, water resources, and environmental systems. These 34 papers were also selected for publication in this book with Digital Object Identifier (DOI) references. We believe that this book will provide the readers with an overview of recent advances in the fields of geospatial technologies and earth resources.

We would like to thank all members of the organizing and selection committees, all blind peer reviewers, all chairpersons, and invited speakers for their invaluable contributions. We are also thankful to (i) Mr. Phuong Kim Minh—President of Dong Bac Corporation, (ii) Assoc. Prof. Tran Xuan Truong—President of the HUMG University Council, Assoc. Prof. Trieu Hung Truong—Vice-Rector of HUMG for

their administrative work and financial supports. Special thanks are also to Doris Bleier and Viradasarani Natarajan at Springer Nature for supporting book production procedures. Finally, all authors are thankful for their manuscript submissions regardless of whether or not their manuscripts were selected.

Hanoi, Vietnam
June 2022

Long Quoc Nguyen
Luyen Khac Bui
Xuan-Nam Bui
Hai Thanh Tran

Reviewers

Anh Quan Duong, Hanoi University of Mining and Geology, Vietnam
Hoang Bac Bui, Hanoi University of Mining and Geology, Vietnam
Ji Chen, Kyoto University, Japan
Dang Vu Khac, Hanoi National University of Education
Tuyet Minh Dang, Thuy Loi University, Vietnam
Kosta Prodanov Dimitrov, University of Mining and Geology, Sofia, Bulgaria
Mai Dinh Sinh, Le Quy Don Technical University, Vietnam
Cao Dinh Trieu, Institute of Geophysics, Geodynamics Department, Vietnam
Cao Dinh Trong, Institute of Geophysics, Geodynamics Department, Vietnam
Minh Duc Do, Hanoi University of Science, Vietnam
Pham Duc Thang, Vietnam Oil and Gas Group, Vietnam
Nguyen Thanh Duong, Hanoi University of Mining and Geology, Vietnam
Van Hao Duong, Hanoi University of Mining and Geology, Vietnam
Tran Thi Huong Giang, Hanoi University of Mining and Geology, Vietnam
Ropesh Goyal, Indian Institute of Technology Kanpur, India
Thi Hang Ha, Hanoi University of Civil Engineering, Vietnam
Hung Ha, State University of New York at Fredonia, USA
Van Long Hoang, Vietnam Petroleum Institute, Vietnam
Le Hong Anh, Hanoi University of Mining and Geology, Vietnam
Nguyen Huu Hiep, Hanoi University of Mining and Geology, Vietnam
Mo Jialin, National Institute for Environmental Studies, Japan
Fan Jiangtao, Chang'an University, China
Oleg I. Kazanin, Saint-Petersburg Mining University, Russia
Nguyen Khac Long, Hanoi University of Mining and Geology, Vietnam
Hung Khuong The, Hanoi University of Mining and Geology, Vietnam
Duy Thong Kieu, Hanoi University of Mining and Geology, Vietnam
Phu Hien La, Thuy Loi University, Vietnam
Nguyen Lan Chau, University of Transport and Communications, Vietnam
Tomasz Lipecki, AGH University of Science and Technology, Poland
Van Anh Cuong Le, University of Science, Ho Chi Minh City
Tien Dung Le, Hanoi University of Mining and Geology, Vietnam

Valeri Mitkov, University of Mining and Geology, Sofia, Bulgaria
Masoud Monjezi, Tarbiat Modares University, Iran
Thuc Ngo, Mien Tay Construction University, Vietnam
Nguyen Ngoc Thach, Hanoi University of Science, Vietnam
Van Lam Nguyen, Norwegian University of Science and Technology, Norway
Nguyen Ba Duy, Hanoi University of Mining and Geology, Vietnam
Nguyen An, University of Science and Education, Vietnam.
Quoc Dinh Nguyen, Vietnam Institute of Geosciences and Mineral Resources
Thinh Nguyen Van, Hanoi University of Mining and Geology, Vietnam
Pham Nhu Sang, Hanoi University of Mining and Geology, Vietnam
Shishkov Peter, University of Mining and Geology, Sofia, Bulgaria
Nguyen Quang Minh, Hanoi University of Mining and Geology, Vietnam
Vo Thi Hanh, Hanoi University of Mining and Geology, Vietnam
Doan Thi Ngoc Hien, Hanoi University of Science and Technology, Vietnam
Bui Tien Dieu, University College of Southeast Norway, Norway
Nguyen Tien Thanh, Hanoi University of Natural Resources and Environment, Vietnam
Hong Hanh Tran, Hanoi University of Mining and Geology, Vietnam
Dinh Trong Tran, Hanoi University of Civil Engineering, Vietnam
Van Anh Tran, Hanoi University of Mining and Geology, Vietnam
Quoc Cuong Tran, Institute of Geological Sciences, Vietnam
Le Hung Trinh, Le Quy Don Technical University, Vietnam
Stanislav Tsvetkov, University of Mining and Geology, Sofia, Bulgaria
Nguyen Van Duc, Korea Institute of Geosciences and Mineral Resources, South Korea
Nguyen Van Sang, Hanoi University of Mining and Geology, Vietnam
Vu Dinh Toan, Université de Toulouse, Toulouse, France

Contents

Application of Unmanned Aerial Vehicles for Surveying and Mapping in Mines: A Review 1
Long Quoc Nguyen, Minh Tuyet Dang, Luyen K. Bui, Quy Bui Ngoc, and Truong Xuan Tran

Mining-Induced Land Subsidence Detected by Persistent Scatterer InSAR: Case Study in Pniówek Coal Mine, Silesian Voivodeship, Poland 23
Thi Thu Huong Kim, Hong Ha Tran, Tuan Anh Phan, and Tomasz Lipecki

Slope Stability Evaluation of Fenghuangshan Landfill Under Rainfall Condition: A Case Study 43
Yuru Chen, Jun Kuang, Renmin Zhu, Jianlin Cao, Jun Zhou, and Qiang Tang

Forecasting PM10 Concentration from Blasting Operations in Open-Pit Mines Using Unmanned Aerial Vehicles and Adaptive Neuro-Fuzzy Inference System 59
Xuan-Nam Bui, Chang Woo Lee, and Hoang Nguyen

Assessing the Effect of Open-Pit Mining Activities and Urbanization on Fine Particulate Matter Concentration by Using Remote Sensing Imagery: A Case Study in Binh Duong Province, Vietnam 75
Thanh Dong Khuc, Long Quoc Nguyen, Dinh Trong Tran, Van Anh Tran, Quynh Nga Nguyen, Xuan Quang Truong, and Hien Quang Pham

Effect of Loading Frequency on the Liquefaction Resistance of Poorly Graded Sand 95
Sung- Sik Park, Dong- Kiem -Lam Tran, Tan-No Nguyen, Seung-Wook Woo, and Hee -Young Sung

An Automatic Method for Clay Minerals Extraction from Landsat 8 OLI Data. A Case Study in Chi Linh City, Hai Duong Province 105
Trinh Le Hung, Nguyen Sach Thanh, and Vuong Trong Kha

Evaluation of the Precision of SARAL/AltiKa and Sentinel-3A Satellite Altimetry Data Over the Vietnam Sea and Its Surroundings ... 121
Do Van Mong, Nguyen Van Sang, Khuong Van Long, and Luyen K. Bui

Detection of GNSS-TEC Noise Related to the Tonga Volcanic Eruption Using Optimization Machine Learning Techniques and Integrated Data 137
Nhung Le, Benjamin Männel, Luyen K. Bui, Mihaela Jarema, Thai Chinh Nguyen, and Harald Schuh

Stability of Road Embankments on Weak Soils 159
Rafail Rafailov

Indirect Georeferencing in Terrestrial Laser Scanning: One-Step and Two-Step Approaches 171
Dung Trung Pham, Long Quoc Nguyen, Tinh Duc Le, and Ha Thanh Tran

Technological Solutions for Fly Ash and Red Mud Upcycling Approach the Vietnam's Government Target of Net-Zero Carbon by 2050 187
Van-Duc Nguyen, Chang-Woo Lee, Xuan-Nam Bui, Pham Van Chung, Quang-Tuan Lai, Hoang Nguyen, Tran Thi Huong Hue, Van-Trieu Do, and Ji-Whan Ahn

Pile–Soil Interaction Mechanism and Optimization Measures Based on Finite Element Method 209
Qi Xu, Remin Zhu, Jianlin Cao, Xuedong Li, Yi Zhang, and Qiang Tang

Determination of Illegal Signs of Coal Mining Expansion in Thai Nguyen Province, Vietnam from a Combination of Radar and Optical Imagery 225
Tran Van Anh, Tran Hong Hanh, Nguyen Quynh Nga, Le Thanh Nghi, Truong Xuan Quang, Khuc Thanh Dong, and Tran Trung Anh

Evaluation of Coal Reserve Reliability in the Nui Beo Mine, Quang Ninh Province Based on the Statistical and Stable Random Function Methods 243
Khuong The Hung, Vu Thai Linh, Pham Thanh Tinh, and Nguyen Khac Duc

Chromite Ore Modeling Based on Detailed Gravity Method in Pursat, Cambodia 259
Trong Cao Dinh, Hung Pham Nam, Thanh Duong Van, Luc Nguyen Manh, Bach Mai Xuan, Trieu Cao Dinh, and Hung Luu Viet

Relationship Between Shear Wave Velocity and Soil Depth and Evaluation of Soil Liquefaction in Quaternary Sedimentary Layer 277
Yu Zhou, Xuedong Li, Yi Zhang, Yibin Li, Xiaoyong Zhang, and Qiang Tang

Characterization of the Natural Dolomite from Thanh Liem Area, Vietnam, and Its Applications 291
Nguyen Thi Thanh Thao, Le Thi Duyen, and Phenglilern Sensousit

A Mine Production Tracking Platform and Its Initial Application in the Digital Transformation for a Vietnamese Coal Exploitation Company 303
Dinh-Van Nguyen, Trung-Kien Dao, Viet-Tung Nguyen, Cong-Dinh Dinh, Trung-Kien Nguyen, Nguyen Quynh Nga, and Chu Thi Khanh Ly

Shear Strength of Poorly Graded Granular Material in Multi-Stage Direct Shear Test 315
Sung-Sik Park, Tan-No Nguyen, Dong-Kiem-Lam Tran, Keum-Bee Hwang, and Hee-Young Sung

High-Resolution Seismic Reflection Survey of Young Sediment at Can Gio Coast, Ho Chi Minh City, Vietnam 325
Thuan Van Nguyen, Cuong Van Anh Le, and Man Ba Duong

Analysis of Geological Structures by 2D Magnetotelluric Inversion in Bang Hot Spring Area, Quang Binh Province 339
Cuong Van Anh Le, Duy Thong Kieu, Ngoc Dat Pham, and Hop Phong Lai

Physicochemical Characteristics of the Middle Triassic Limestone in Ha Nam Province, Vietnam and the Ability of Adsorption of Heavy Metal Ions from Aqueous Environments 357
Bui Hoang Bac, Le Thi Duyen, Nguyen Thi Thanh Thao, and Nguyen Huu Tho

Local Mechanical Behaviors of Steel Box Girder During Skew Incremental Launching 371
Jiabao Du, Wen Niu, Yu Shi, Yongzhe Wu, Yuan Chen, and Qiang Tang

GIS Applications in Land Adaptability Mapping for Perennial Industrial Crops in Nghe An Province, Vietnam 383
Hanh Thi Tong, Kien-Trinh Thi Bui, Cuong Manh Nguyen, and Yit Chanthol

Land-Use and Land-Cover Change Detection and Classification to Analyze Dynamics of Dragon Fruit Farming in Sand Dunes Area of Binh Thuan Province of Vietnam 405
Luan Hong Pham, Trong Dieu Hien Le, Lien T. H. Pham, Ho Nguyen, and Hong Quan Nguyen

Random Forest Analysis of Land Use and Land Cover Change Using Sentinel-2 Data in Van Yen, Yen Bai Province, Vietnam 429
Xuan Quang Truong, Nguyen Hien Duong Dang, Thi Hang Do, Nhat Duong Tran, Thi Thu Nga Do, Van Anh Tran, Vasil Yordanov, Maria Antonia Brovelli, and Thanh Dong Khuc

Engineering Geological Problems of Foundation Pit Construction in Quaternary Strata: Taking Suzhou Area as an Example 447
Xinyu Luo, Peng Yin, Yongsheng Zheng, Xuedong Li, Yi Zhang, and Qiang Tang

Roof Condition Characteristics Affecting the Stability of Coal Pillars and Retained Roadway 463
Quang Phuc Le and Van Chi Dao

On the Flow Assurance for Un-Insulated Subsea Pipeline Systems: Application on the Multiphase Pipeline from Pearl Field to FPSO Ruby II Offshore Vietnam 479
Van Thinh Nguyen, Thi Hai Yen Nguyen, Sylvain S. Guillou, Thuy Huong Duong, Thi Thanh Thuy Truong, and Thi Thao Nguyen

Detection of Underground Anomalies by Evaluation of Ground Penetrating Radar Attribute Combination 495
Duy Hoang Dang, Cuong Van Anh Le, and Thuan Van Nguyen

Dynamic Failure Process of Soil Particles at the End of Shield Tunnel Based on Discrete Element 509
Zheyuan Feng, Bin Liu, Sijun Zhang, Fei Kang, Haipeng Hui, and Qiang Tang

Early Triassic Tectonic Evolution of the Northeastern Kontum Massif: New Constraints from the S-type Granite in Ba To Area, Quang Ngai Province, Central Vietnam 521
Hai Thanh Tran, Bui Vinh Hau, Ngo Xuan Thanh, Nguyen Huu Hiep, and Ngo Thi Kim Chi

Proposal of Study on InSAR-Based Land Subsidence Analysis as Basis for Subsequent Hydro-mechanical Modeling: A Case Study of Hanoi, Vietnam 535
Hong Ha Tran, Luyen K. Bui, Hung Q. Ha, Thi Thu Huong Kim, and Christoph Butscher

Evaluation of the Precision of SARAL/AltiKa and Sentinel-3A Satellite Altimetry Data Over the Vietnam Sea and Its Surroundings

Do Van Mong, Nguyen Van Sang, Khuong Van Long, and Luyen K. Bui

Abstract Satellite altimetry has proven to be a useful tool to measure sea surface height, which is of diverse applications in oceanography, geodesy, among others. However, the precision of satellite altimetry data is different between missions and areas. This article evaluates the precision of observed data received by two satellite altimeters of SARAL/AltiKa and Sentinel-3A in the Exact Repeat Mission mode over the Vietnam Sea and its surroundings. The precision of the data is assessed based on height differences at intersection points between ascending and descending tracks. First, the positions of each intersection point between the ascending and descending tracks are interpolated from measure points with the second-order polynomial model. Then, the standard deviation of the height difference is estimated from all intersection points for each of 34 repeat cycles (SARAL/AltiKa) and 28 repeat cycles (Sentinel-3A) over the study area. The results show that the standard deviations of the SARAL/AltiKa data are between ± 4.5 cm and ± 7.5 cm, with an average of ± 5.9 cm, while those of Sentinel-3A range from ± 4.4 cm to ± 7.7 cm, with an average of ± 5.9 cm. Of both datasets, the height differences are greater at points located close to the coastlines and islands.

Keywords Satellite altimetry · SARAL · AltiKa · Sentinel-3A · Vietnam Sea

D. Van Mong · K. Van Long
Vietnam's People Naval Hydrographic and Oceanographic Department, Hai Phong 04000, Vietnam

N. Van Sang (✉) · L. K. Bui
Faculty of Geomatics and Land Administration, Hanoi University of Mining and Geology, Hanoi 100000, Vietnam
e-mail: nguyenvangsang@humg.edu.vn

L. K. Bui
e-mail: buikhacluyen@humg.edu.vn

L. Q. Nguyen et al. (eds.), *Advances in Geospatial Technology in Mining and Earth Sciences*, Environmental Science and Engineering,
https://doi.org/10.1007/978-3-031-20463-0_8

1 Introduction

Starting from the 1980s, satellite altimeter has been developed rapidly and become a useful tool for marine research. Since the first satellite platform Geodetic/Geophysical Satellite (Geosat) was launched in 1985, there have been many satellite missions working on their orbits; 10 inactive satellite missions are Geosat, the European Remote Sensing satellite (ERS-1/2), TOPEX/Poseidon (T/P), the US navy Geosat Follow On (GFO), Jason-1/2, Environmental Satellite (Envisat), Hai Yang 2A (HY-2A), Satellite pour l'Observation de la Terre (SPOT), and 9 active satellite missions being CryoSat, SARAL/AltiKa, Jason-3, Sentinel-3A/B, Chinese-French Oceanography Satellite (CFOSAT), HY-2B/2C, Jason-CS. The Surface Water and Ocean Topography (SWOT) satellite mission was scheduled to be launched in 2022. The satellites have created a rich database that has been applied in various fields, such as oceanography, hydrology, land and coastal studies, ice and cryosphere, climate, atmosphere, wind and waves, geodesy, and geophysics [1]. Satellite altimeters data are available in the exact repeat mission (ERM) or geodetic mission (GM) mode. In the ERM mode, the observations are made repeatedly at a regular time interval but with a low spatial resolution. This kind of data is useful for oceanography and climate sciences, but not applicable for the determination of high-resolution gravity field modeling. The data received from the geodetic mission (GM) can be used for various applications in geodesy. In this mode, the satellite flies in a non-repeated orbit where the observations are taken once only at each location, but with a much higher spatial density [2].

In the Vietnam Sea and the surrounding area, bounded by [5°N, 25°N] in latitude and [105°E, 120°E] in longitude, there have been several studies applying satellite altimeter data. For example, in 2000, Hwang et al. [3] used the Topex/Poseidon satellite altimeter data to determine surface currents in the East Sea. In 2012, marine gravity anomalies were determined from the ENVISAT data combined with *in-situ* gravity data measured at the coast and islands in the East Sea, in which an accuracy of about ± 6 mGal was obtained [4]. In 2019, Tran et al. improved the accuracy of marine gravity anomalies derived from satellite altimetry by fitting with the ship-derived gravity anomaly in the East Sea. The results showed the accuracy of the gravity anomaly from ± 1.21 to ± 9.36 mGal [5]. In 2020, the accuracies of the global gravity anomaly models DTU10GRAV, DTU13GRAV, DTU15GRAV were evaluated in the Vietnam Sea by comparing with ship-derived gravity anomaly data, which were found to be ± 5.80, ± 5.73, and ± 5.63 mGal, respectively [6]. Also in 2020, the marine gravity anomaly over the Gulf of Tonkin was determined from the CryoSat-2 and SARAL/AltiKa satellite altimeter data with the accuracies achieved before and after fitting with shipborne gravity data being ± 3.36 and ± 2.63 mGal, respectively [7]. These studies indicated that satellite altimeter data are of great interest in the study area.

The precision of satellite altimetry data is different between missions and study areas [2], depending on the characteristics of the sea, the corrections to the satellite altimeter data according to the global correction models, which may not be accurate

enough for regional areas. Therefore, it is necessary to evaluate the precision of satellite altimeter data at the regional scale before applying them. As a result, several studies have been conducted to evaluate the precision of satellite altimeter data. For instance, in 2012, altimetric sea levels in coastal areas were validated using available tide gage records in the Nordic, Barents, and Kara seas [8]. The comparison results showed that, at most locations in the Nordic Sea, the satellite altimeter data are in good agreement with the tide gage data, but the agreement is low at the shallows of the Barents and Kara Seas due to the seasonal presence of sea ice [8]. In 2017, the main range and geophysical corrections of TOPEX/Poseidon, Jason-1, and Jason-2 satellite altimetry data were evaluated over the Indonesian Sea, in which the distances from the coast at altimeter crossovers were used to assess the quality of the various corrections and mean sea surface models [9]. Also in 2017, the precision of CryoSat-2 satellite altimeter data was evaluated in the waters around the Spratly Islands, Vietnam, in which the results showed that the precision of CryoSat-2 satellite altimeter data from periods 31 to 43 is $\pm$ 3.5 cm [10]. Location and height difference at crossover points in satellite altimetry data processing were determined using a direct method in 2017 [11]. In 2020, Sentinel-3A and Jason-3 satellite data in the coastal area of the European Sea were evaluated by comparison with tide gage measurements, with the results showing that the root mean square deviation (RMSD) of Sentinel-3A is 13% lower than that of the Jason-3 [12].

Sentinel-3A was launched on February 16, 2016, and is now working in the ERM mode. As a result, its measurements are suitable for studying ocean currents. The mission measurements have been collected since March 12, 2016, with a repeated cycle of 27 days [13]. The SARAL/AltiKa satellite, a product made under the cooperation between the Indian Space Research Organization (ISRO) and Centre national d'études spatiales (CNES), was launched on February 25, 2013. The SARAL/AltiKa satellite collected the measurements in the ERM mode from March 14, 2013, to July 4, 2016, with a repeated cycle of 35 days, which is suitable for studying ocean currents. It then changed into the GM mode from July 4, 2016 onward, which is suitable for gravity field research [14].

Up to now, there have no studies on the assessment of the precision of the SARAL/AltiKa or Sentinel-3A data over the Vietnam Sea and its surroundings. This paper conducts an evaluation of the precision of their data based on height differences at intersection points between the ascending and descending tracks and experimentally evaluates the precision of the SARAL/AltiKa and Sentinel-3A data in the ERM mode. The research is a preliminary step in a further planned project to apply the SARAL/AltiKa and Sentinel-3A satellite altimeter data in studying the ocean current over the Vietnam Sea and its surroundings.

2 Research Area and Data

2.1 Research Area

The study area is the Vietnam Sea and the surrounding area, bounded by [5°N, 25°N] in latitude and [105°E, 120°E] in longitude (Fig. 1). In this area, tides, waves, and currents vary significantly, which affect the precision of the corrections in the satellite altimeter data. The sea of Vietnam and the surrounding area is an area with different tidal regimes; in the North, the tidal regime is the regular diurnal tide. In the Central region, there is an irregular diurnal tide. In the South, the tidal regime is quite complicated from semi-diurnal to diurnal tide with large tidal amplitudes [15].

The surface current in the East Sea area is clearly shown by the seasonal regime and two large-scale vortices. The winter current system is dominated by the prevailing wind field in the area and partly influenced by the geomorphic current system caused by temperature fields and sea salinity. In addition, the most prominent feature of the surface current in this period is the presence of a large cyclone over the entire sea [16]. For the surface laminar current system, which is formed mainly by the southwest wind field, with the characteristics of being strongly differentiated by the impact of the tropical convergence band. In addition, with the intensification of warm waters according to the deep sea off the Southeast, anti-vortexes which counterbalance with winter vortexes have been formed [17].

The wave height properties of this area are also extremely diverse. The smallest wave height is less than 3 m and located in the western part of the Gulf of Thailand. The area with the highest wave height of more than 12 m can be found in the northeast area of the East Sea due to frequent storm and strong northeast wind activities. The central area of the Gulf of Tonkin has the highest wave height of about 9–10 m. The central area of the East Sea has the highest wave height of about 11 m [18].

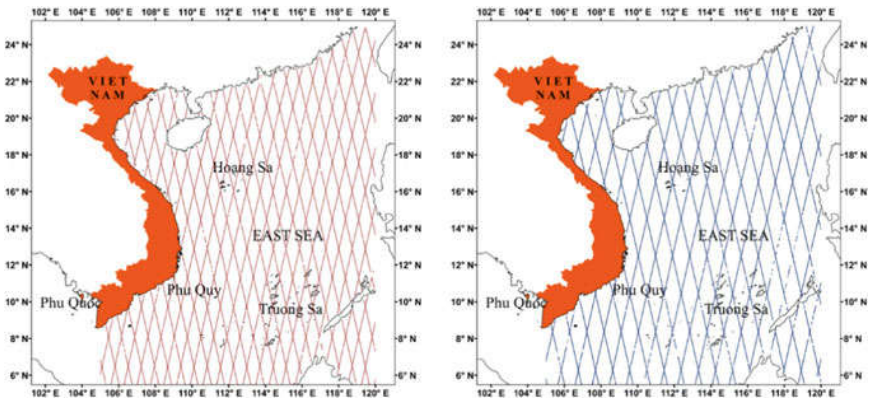

Fig. 1 Track distribution of SARAL/AltiKa (left) and Sentinel-3A (right) satellites

The composition of marine life in this area is of the tropical nature that mainly consists of tropical species distributed in the Western Indo-Pacific region. In addition, in the northern border region of Vietnam, where the tropical monsoon climate is cold, there are also a number of subtropical species distributed from the subtropical China Sea. In terms of ecology, the East Sea is also extremely diverse, with typical ecosystems such as submerged forests, coral reefs, and seagrasses [18].

2.2 Research Data

The data used in this study are obtained from two satellite altimeter systems of SARAL/AltiKa and Sentinel-3A in the ERM measurement mode, within the spatial limit from 5 to 25°N in latitude and from 105 to 120°E in longitude. These data are provided by the Radar Altimeter Database System [19].The SARAL/AltiKa data were collected and aggregated over 34 cycles (from 1st cycle to 34th cycle), corresponding to a measurement period of over 3 years (from March 14, 2013, to June 16, 2016) with a total of 306,223 measurement points. Figure 1 (left) shows the track distribution of the SARAL/AltiKa satellite.

The Sentinel-3A data were collected and aggregated over 28 cycles (from 48th cycle to 75th cycle) in the ERM mode, corresponding to a time span of over 2 years (from August 7, 2019, to September 2, 2021) with a total of 306,223 measurement points. Figure 1 (right) shows the track distribution of the Sentinel-3A satellite. The information regarding the used data is summarized in Table 1. The corrections used in calculating sea surface height (SSH) include orbit, dry and wet tropospheric, ionospheric, solid earth tide, ocean tide, load tide, pole tide, and sea state bias [19].

Table 1 Summary of collected satellite altimeter data

Data	Repeat cycle (day)	Number of cycles	Measurement time	Measurement points
SARAL/AltiKa	35	34	from March 14, 2013, to June 16, 2016	306,223
Sentinel-3A	27	28	from August 7, 2019, to September 2, 2021	210,375
Total		62		516,598

3 Precision Evaluation

3.1 Locating and Computing the Height Difference at the Intersection

According to the operating principle of satellite altimeter systems, when encountering sea water, the wave beams from the satellite reflect back to the receivers on the satellites. The tracks can be classified into ascending and descending tracks. The intersection of the ascending and descending tracks forms the intersection points. The analysis of data sources received from the SARAL/AltiKa and Sentinel altimeter satellites shows that the position of the intersection point between the arcs formed from the dataset often does not coincide with the location of the received data points. Therefore, in order to evaluate the accuracy of satellite altimeter data, the research task requires determining the exact positions of the intersection points and computing the differences in sea level in these positions [20]. In the research content, we use the second-order polynomial simulation method to solve the above two problems [21]. Suppose on a data track, the point has coordinates of (ϕ_i, λ_i). This track will be simulated by a quadratic polynomial [21]:

$$\lambda = a\varphi^2 + b\varphi + c \tag{1}$$

where a, b, c are the parameters to be determined, in which at least three known coordinate points (i.e., the data points from the altimeter satellites over the track) are required. If there are more than three points, then the parameters are determined according to the principle of least squares.

If the ascending track is simulated by a polynomial model by:

$$\lambda = a_a\varphi^2 + b_a\varphi + c_a \tag{2}$$

And the descending track is simulated by a polynomial model by:

$$\lambda = a_d\varphi^2 + b_d\varphi + c_d \tag{3}$$

Then, the position of the intersection point is the solution of the system of equations:

$$\begin{cases} \lambda = a_a\varphi^2 + b_a\varphi + c_a \\ \lambda = a_d\varphi^2 + b_d\varphi + c_d \end{cases} \tag{4}$$

The system of Eqs. (4) has two solutions, that is, there will be two intersection points located in the two halves of the parabolic graph of the quadratic polynomial. The intersection point is detected based on the beginning and the ending points of the track. Comparing these two points with the beginning and the end points of the track

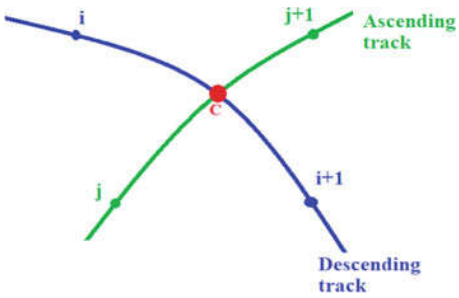

Fig. 2 Exact intersection location

helps to find a suitable intersection. The position of the found intersection point is not an exact location, but an approximate location. After determining an approximate intersection point, four neighborhood points of the intersection i, $i + 1$, j, and $j + 1$ from the ascending and descending tracks are determined (Fig. 2). From these 4 points, we will determine the position of the intersection point (C) more accurately.

After the position of the intersection is determined, the SSH at the intersection point according to the ascending track $(\mathrm{SSH}_{C,a})$ and the descending track $(\mathrm{SSH}_{C,d})$ will be interpolated from neighboring measurement points i, $i + 1$, j, and $j + 1$. The height difference at the intersection point is computed by:

$$\mathrm{dH} = \mathrm{SSH}_{C,a} - \mathrm{SSH}_{C,d} \tag{5}$$

3.2 *Evaluating the Precision of Satellite Altimeter Data Based on the Height Differences at the Intersection Points*

$\mathrm{SSH}_{C,a}$ and $\mathrm{SSH}_{C,d}$ are the SSHs at the intersection point C computed according to the two ascending and descending tracks. If there is no error, then the two values are identical (i.e., $\mathrm{dH} = 0$). In fact, the value of $\mathrm{dH} \neq 0$ is due to measurement errors (Fig. 3). Therefore, based on the dH value at the intersection point, we can evaluate the altimeter satellite measurement accuracy.

Let dH_i be the measured value at the i-th intersection. Over the entire study area, we have a series of measurement values $(\mathrm{dH}_1, \mathrm{dH}_2, \ldots, \mathrm{dH}_m)$. The true values of these measurements are all zero. The mathematical expectation of this range of values is calculated by:

$$E(\mathrm{dH}) = \overline{\mathrm{dH}} = \frac{[\mathrm{dH}]}{m} \tag{6}$$

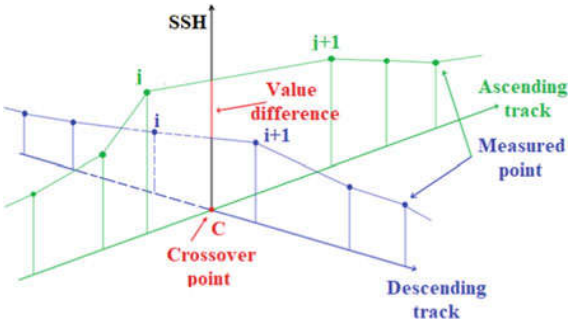

Fig. 3 Height difference at the intersection

+If the mathematical expectation E(dH) = 0, then there is no systematic error in the measurements, then the precision of the measured values is determined by:

$$\mathrm{RMS}_{\mathrm{dH}} = \pm\sqrt{\frac{[\mathrm{dH}.\mathrm{dH}]}{m}} \tag{7}$$

According to the principle of equal influence, from Eq. (5), we have:

$$\mathrm{RMS}_{\mathrm{dH}}^2 = \mathrm{RMS}_a^2 + \mathrm{RMS}_d^2 = 2\mathrm{RMS}_{\mathrm{SSH}}^2 \tag{8}$$

Substituting to Eq. (7), we have:

$$\mathrm{RMS}_{\mathrm{SSH}} = \frac{\mathrm{RMS}_{\mathrm{dH}}}{\sqrt{2}} = \pm\sqrt{\frac{[\mathrm{dHdH}]}{2m}} \tag{9}$$

+If the mathematical expectation E(dH) ≠ 0, then there is systematic error in the measurements, and the precision of the measured values is determined according to the standard deviation by the Bessel equation:

$$\mathrm{STD}_{\mathrm{dH}} = \pm\sqrt{\frac{[vv]}{m-1}} \tag{10}$$

where given is the calculated correction:

$$v = \mathrm{dH} - \overline{\mathrm{dH}}$$

Then, the precision of the SSH is determined by:

$$\mathrm{STD}_{\mathrm{SSH}} = \frac{\mathrm{STD}_{\mathrm{dH}}}{\sqrt{2}} = \pm\sqrt{\frac{[vv]}{2(m-1)}} \tag{11}$$

4 Results of Precision Evaluation of SARAL/Altika and Sentinel-3A Data in the Waters of Vietnam and Surrounding Areas

4.1 Results of Precision Evaluation of the SARAL/Altika Satellite Altimeter Data

In this section, we evaluate the precision of the SARAL/AltiKa satellite altimeter data for 34 cycles with the results shown in Table 2, Figs. 4 and 5.

The results in Table 2 show that, over the study area, the standard deviations of the SARAL/AltiKa data are between ± 4.5 cm and ± 7.5 cm, with an average of ± 5.9 cm. The average deviation at the intersections is small, ranging from − 0.033 m to 0.004 m. This indicates that the systematic error in the SARAL/AltiKa satellite altimeter data over study area is small.

4.2 Results of Precision Evaluation of Sentinel-3A Satellite Altimeter Data

The results of precision evaluation of Sentinel-3A satellite altimeter data are shown in Table 3, Figs. 6 and 7.

Maximum, minimum, and average values of precision of the Sentinel-3A satellite altimeter data are ± 4.4 cm, ± 7.7 cm, and ± 5.9 cm, respectively. The average deviation at the intersection is small, ranging from − 0.022 m to 0.023 m. This proves that the systematic error in the Sentinel-3A satellite altimeter data is small over the study area.

In order to identify the areas with large height differences at the intersections (dH), we show the average height difference of all cycles of the SARAL/AltiKa satellite in Fig. 8 and the Sentinel-3A satellite in Fig. 9. The results for both data show that the height differences are larger at points located close to the coastlines and islands. Additionally, Fig. 9 shows that not only in the coastal zones, large SSH differences at the intersections can also be found in the area between the Hoang Sa and Truong Sa Islands. This is likely that, in this area, the corrections to the satellite altimeter data according to the global correction models are not very appropriate. It is necessary to study and correct local factors to improve the precision of satellite altimeter data in these areas.

Table 2 Results of evaluating of the precision of the SARAL/AltiKa satellite altimeter data

Cycle	Number of intersection	$\mathbf{dH_{max}}$ (m)	$\mathbf{dH_{min}}$ (m)	$\mathbf{dH_{mean}}$ (m)	$\mathbf{RMS_{SSH}}$ (m)	$\mathbf{STD_{SSH}}$ (m)
CK01	169	0.393	− 0.949	− 0.001	0.075	0.075
CK02	149	0.217	− 0.311	0.000	0.050	0.050
CK03	129	0.482	− 0.225	− 0.007	0.060	0.060
CK04	153	0.225	− 0.331	− 0.011	0.059	0.058
CK05	156	0.204	− 0.314	− 0.003	0.055	0.055
CK06	155	0.542	− 0.377	− 0.016	0.075	0.074
CK07	172	0.374	− 0.301	0.004	0.073	0.073
CK08	165	0.428	− 0.22	− 0.007	0.066	0.066
CK09	174	0.471	− 0.347	− 0.033	0.072	0.064
CK10	170	0.281	− 0.259	− 0.004	0.058	0.058
CK11	178	0.208	− 0.236	− 0.006	0.050	0.050
CK12	140	0.199	− 0.214	0.003	0.046	0.046
CK13	136	0.258	− 0.273	− 0.013	0.054	0.053
CK14	161	0.367	− 0.282	− 0.013	0.061	0.059
CK15	164	0.319	− 0.189	0.004	0.057	0.057
CK16	142	0.244	− 0.251	− 0.006	0.054	0.053
CK17	108	0.287	− 0.266	− 0.014	0.070	0.068
CK18	170	0.322	− 0.220	0.002	0.056	0.056
CK19	171	0.483	− 0.325	− 0.024	0.074	0.070
CK20	179	0.186	− 0.284	− 0.021	0.056	0.052
CK21	169	0.165	− 0.193	− 0.012	0.047	0.045
CK22	172	0.413	− 0.280	− 0.017	0.057	0.054
CK23	146	0.196	− 0.264	− 0.006	0.049	0.049
CK24	138	0.355	− 0.301	0.001	0.065	0.065
CK25	135	0.287	− 0.385	− 0.015	0.060	0.058
CK26	149	0.278	− 0.349	− 0.011	0.061	0.061
CK27	146	0.468	− 0.324	− 0.005	0.074	0.074
CK28	162	0.349	− 0.269	− 0.018	0.059	0.056
CK29	165	0.273	− 0.450	− 0.001	0.067	0.066
CK30	178	0.304	− 0.408	− 0.024	0.073	0.069
CK31	177	0.309	− 0.295	− 0.009	0.056	0.056
CK32	171	0.292	− 0.232	− 0.007	0.050	0.050
CK33	154	0.220	− 0.282	− 0.005	0.053	0.053
CK34	153	0.343	− 0.381	− 0.010	0.059	0.058
Max	179	0.542	− 0.189	0.004	0.075	0.075
Min	108	0.165	− 0.949	− 0.033	0.046	0.045

(continued)

Table 2 (continued)

Cycle	Number of intersection	dH_{max} (m)	dH_{min} (m)	dH_{mean} (m)	RMS_{SSH} (m)	STD_{SSH} (m)
Mean	157.5	0.316	− 0.311	− 0.009	0.060	0.059

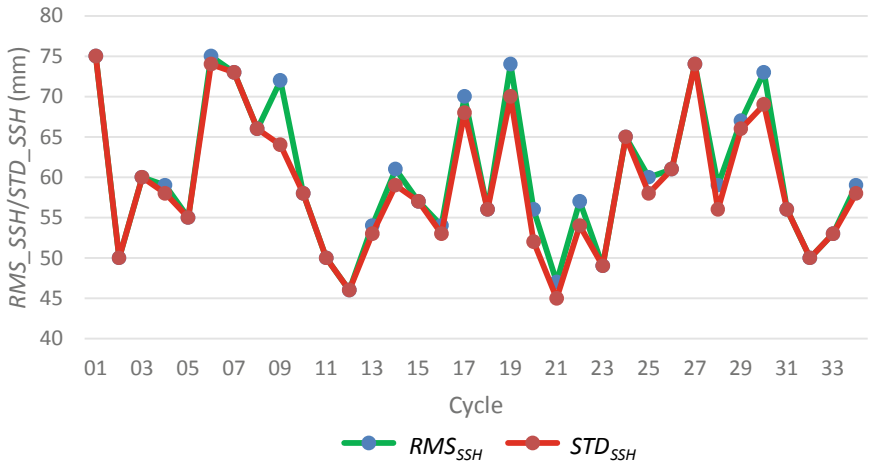

Fig. 4 RMS_{SSH} and STD_{SSH} of SARAL/AltiKa satellite data for 34 cycles

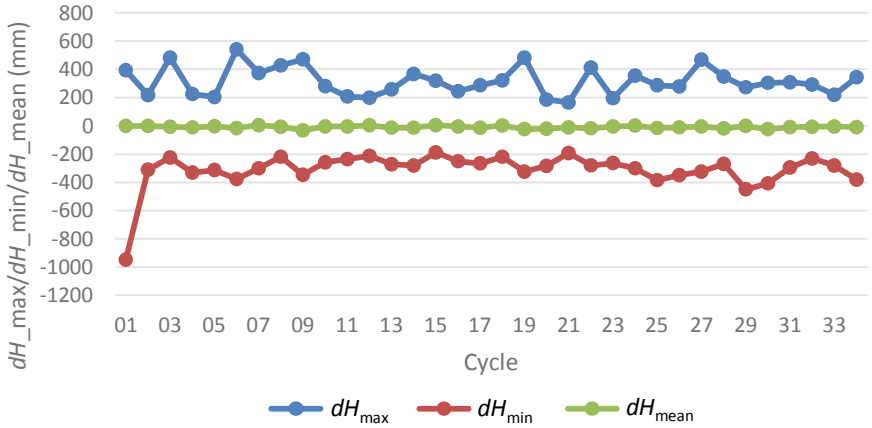

Fig. 5 dH_{max}, dH_{min}, and dH_{mean} of SARAL/AltiKa satellite data for 34 cycles

Table 3 Results of evaluating the precision of Sentinel-3A satellite altimeter data

Cycle	Number of intersection	$\mathbf{dH_{max}}$ (m)	$\mathbf{dH_{min}}$ (m)	$\mathbf{dH_{mean}}$ (m)	$\mathbf{RMS_{SSH}}$ (m)	$\mathbf{STD_{SSH}}$ (m)
CK48	110	0.185	− 0.315	− 0.016	0.057	0.055
CK49	111	0.266	− 0.280	0.007	0.061	0.061
CK50	108	0.725	− 0.217	0.023	0.078	0.075
CK51	113	0.379	− 0.225	0.016	0.069	0.067
CK52	108	0.247	− 0.292	0.013	0.071	0.070
CK53	110	0.247	− 0.735	0.011	0.078	0.077
CK54	114	0.185	− 0.264	0.014	0.056	0.054
CK55	114	0.193	− 0.255	0.003	0.059	0.059
CK56	114	0.372	− 0.324	0.008	0.060	0.059
CK57	113	0.259	− 0.195	0.005	0.051	0.051
CK58	107	0.268	− 0.154	− 0.002	0.056	0.056
CK59	102	0.160	− 0.223	− 0.014	0.052	0.050
CK60	106	0.256	− 0.306	− 0.021	0.060	0.057
CK61	103	0.248	− 0.211	− 0.010	0.062	0.061
CK62	101	0.135	− 0.220	− 0.017	0.049	0.046
CK63	100	0.215	− 0.390	0.002	0.059	0.059
CK64	107	0.271	− 0.302	0.004	0.070	0.070
CK65	110	0.178	− 0.387	0.012	0.062	0.061
CK66	108	0.288	− 0.477	0.022	0.067	0.064
CK67	111	0.201	− 0.193	0.004	0.059	0.059
CK68	112	0.538	− 0.236	0.005	0.062	0.062
CK69	110	0.214	− 0.237	0.006	0.049	0.049
CK70	109	0.337	− 0.171	0.012	0.054	0.052
CK71	108	0.131	− 0.316	− 0.021	0.057	0.053
CK72	104	0.203	− 0.236	− 0.016	0.047	0.044
CK73	108	0.269	− 0.209	− 0.017	0.058	0.055
CK74	109	0.424	− 0.272	− 0.008	0.064	0.063
CK75	104	0.200	− 0.244	− 0.022	0.060	0.056
Max	114	0.725	− 0.154	0.023	0.078	0.077
Min	100	0.131	− 0.735	− 0.022	0.047	0.044
Mean	108.4	0.271	− 0.282	0.000	0.060	0.059

5 Conclusion

This paper has presented the evaluation of the precision of SARAL/AltiKa and Sentinel-3A satellite altimeter data over the Vietnam Sea and surroundings based on height differences at the intersection points. The evaluation was conducted with

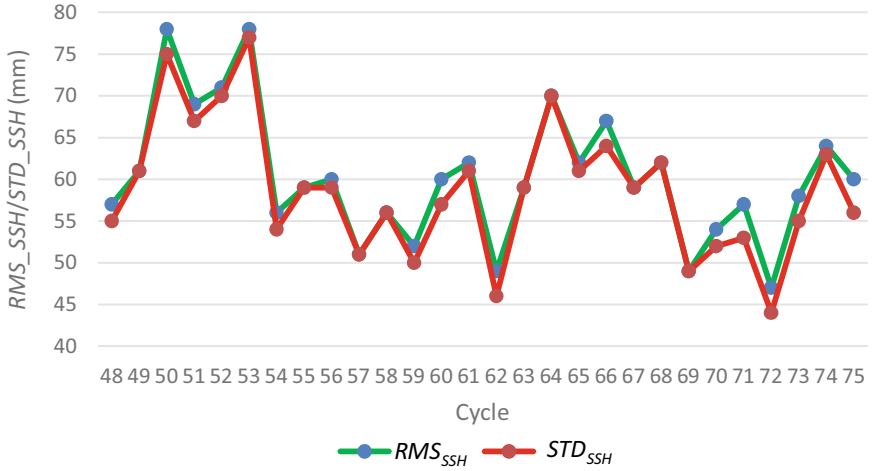

Fig. 6 RMS_{SSH} and STD_{SSH} values of Sentinel-3A satellite data for 28 cycles

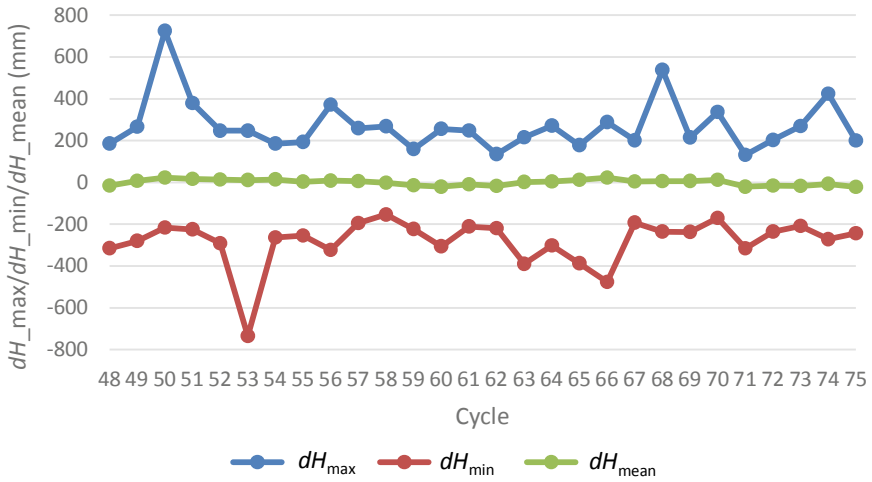

Fig. 7 dH_{max}, dH_{min}, and dH_{mean} values of Sentinel-3A satellite data for 28 cycles

34 cycles of the SARAL/AltiKa satellite data (from 1st to 34th cycle), corresponding to an over 3-year period, and the Sentinel-3A satellite data at 28 cycles (from 48 to 74th cycle), corresponding to a more than 2-year time span. Both evaluations were performed with data in the ERM mode.

The standard deviations of the SARAL/AltiKa data are between ± 4.5 cm and ± 7.5 cm, with an average of ± 5.9 cm, while that of the Sentinel-3A satellite altimeter data was found between ± 4.4 and ± 7.7 cm, with a mean value of ± 5.9 cm. The mean height difference at the intersection points is small indicating a

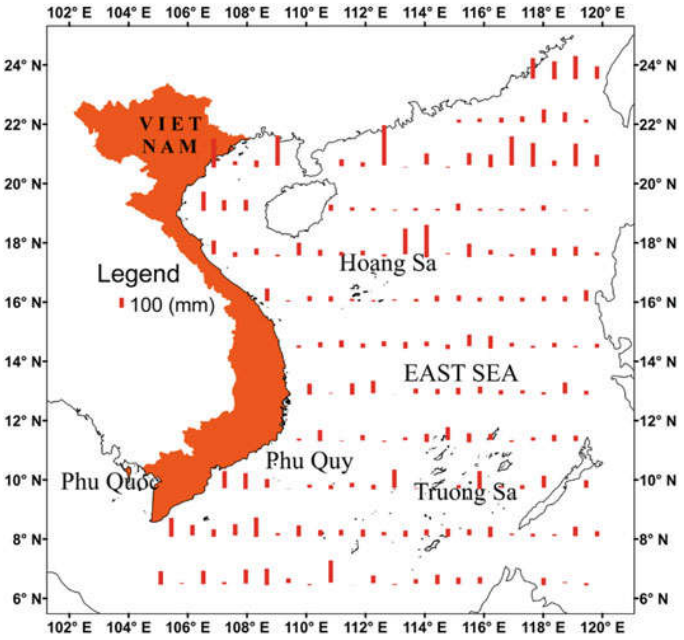

Fig. 8 Height difference (dH) at the intersection points of SARAL/AltiKa satellite

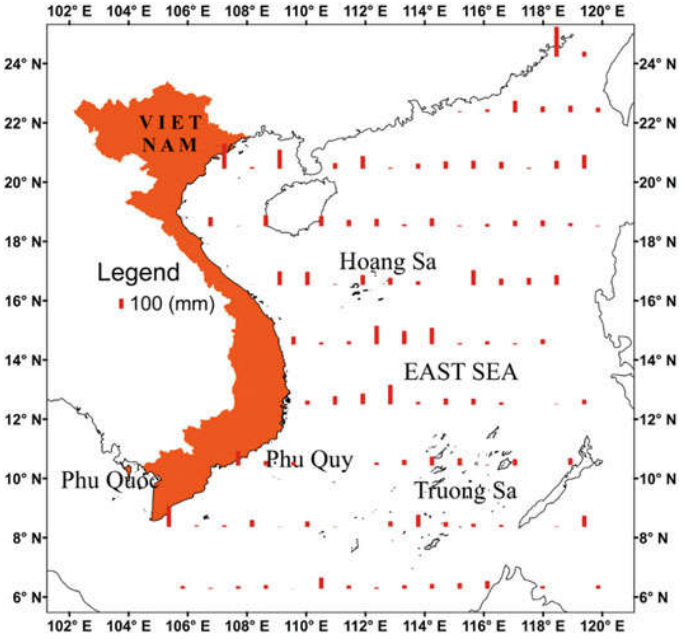

Fig. 9 Height difference (dH) at the intersection points of Sentinel-3A satellite

small systematic error in satellite altimeter data over the study area. Additionally, the height differences at intersection points are found higher in coastal areas and the areas near the archipelagos than those in offshore areas. This difference is also large with Sentinel-3A satellite data in the area between the Hoang Sa and Truong Sa Islands.

Acknowledgements This research has been supported by the project “Research on determining seafloor depth for the East Sea using gravity anomaly data”, code B2021-MDA-06 of the Vietnam Ministry of Education and Training and the project "Research to determine surface currents in the East Sea using satellite altimeter data", code 07/2021/ĐĐ6-DATS of Vietnam’s People Naval Hydrographic and Oceanographic Department. We would also like to thank Radar Altimeter Database System for providing satellite altimeter data used in this study.

References

1. Shum, C.K., Ries, J.C., Tapley, B.D.: The accuracy and applications of satellite altimetry. Geophys. J. Int. **121**, 321–336 (1995)
2. Andersen, O.B.: Marine Gravity and Geoid From Satellite Altimetry. Springer, Geoid Determination (2013)
3. Hwang, C., Chen, S.-A.: Circulations and eddies over the South China Sea derived from TOPEX/POSEIDON altimeter data. J. Geophys. Res. Atmos. **105**, 23 (2000)
4. Nguyen, V.S.: Determination of gravity anomalies for Vietnamese waters by satellite altimeter results, vol. Ph.D.,. Moscow State University of Geodesy and Mapping, Russian Federation (2012)
5. Tran, T.D., Kulinich, R.G., Nguyen, V.S., Bui, C.Q., Nguyen, B.D., Nguyen, K.D., Tran, T.D., Tran, T.L.: Improving accuracy of altimeter-derived marine gravity anomalies for geological structure research in the Vietnam south-central continental shelf and adjacent areas. Russ. J. Pac. Geol. **13**, 11 (2019)
6. Nguyen, V.S.: Evaluation of the accuracy of the global gravity anomaly model determined from satellite altimeter over the East Sea. Min. Ind. J. **4** (2020)
7. Nguyen, V.S., Pham, V.T., Nguyen, V.L., Andersen, B.O., Forsberg, R., Bui, T.D.: Marine gravity anomaly mapping for the Gulf of Tonkin area (Vietnam) using Cryosat-2 and Saral/AltiKa satellite altimetry data. Adv. Space Res. (2020)
8. Volkov, D.L., Pujol, M.I.: Quality assessment of a satellite altimetry data product in the Nordic, Barents, and Kara seas. J. Geophys. Res. **117** (2012)
9. Eko, Y.H., Maria, J.F., Clara, L.: Assessment of altimetric range and geophysical corrections and mean sea surface models—impacts on sea level variability around the Indonesian seas. Remote Sens. **9** (2017)
10. Nguyen, V.S., Vu, V.T.: Evaluation of accuracy of the altimetry data in the sea area around the Truong Sa Archipelago. J. Min. Earth Sci. **58**, 5 (2017)
11. Nguyen, V.L., Nguyen, V.S., Tran, T.T.T., Le, T.T.T.: Determination of location and height difference at crossover points in satellite altimetry data processing using direct method. In: International Conference on Geo-spatial Technologies and Earth Resources, pp. 279–282. Publishing House for Science and Technology (2017)
12. Sánchez-Román, A., Pascual, A., Pujol, M.-I., Taburet, G., Marcos, M., Faugère, Y.: Assessment of DUACS Sentinel-3A altimetry data in the coastal band of the European seas: comparison with tide gauge measurements. Remote Sens. **3970** (2020)
13. ESA. Retrieved from https://sentinels.copernicus.eu/web/sentinel/missions/sentinel-3

14. Verron, J., Bonnefond, P., Aouf, L.: The benefits of the Ka-Band as evidenced from the SARAL/AltiKa altimetric mission: scientific applications. Remote Sens. **163** (2018)
15. Ha, M.H.: Research and assessment of sea level standards according to modern geodetic, hydrographic and tectonic methods for the construction of works and planning of Vietnam's coastal zone in the changing trend climate change. In: General report on results of scientific research and technological development of the project KC.09.19/11–15 (2015)
16. Rong, Z.M.: Analysis on the surface current features in the South China Sea in winter. Mar. Forecast. **B11**, 5 (1994)
17. Xu, X.Z., Qiu, Z., Chen, H.C.: The general descriptions of the horizontal circulation in the South China Sea. In: In Proceedings of the 1980 Symposium on Hydrometeorology of the Chinese Society of Oceanology and Limnology, pp. 137–145. Science Press (1982)
18. Le, D.T.: The Marine management. Hanoi National University of Vietnam (2005)
19. Radar Altimeter Database System. Retrieved from http://rads.tudelft.nl/rads/rads.shtml
20. Nguyen, V.S.: Adjustment of ENVISAT altimetry data crossover for water area adjacent to Vietnam. Geodesy Aerophotogr. **5** (2012)
21. Nguyen, V.S.: Determination crossover point location by simulating quadratic-equation in processing satellite altimetry data. J. Min. Earth Sci. **41**, 5 (2013)